[1, 2.]Fatai Olufemi ARAMIDE, [1.]Okikiola Ganiu AGBABIAKA,
[1.]Luanu AMANABO, [2.]Patricia Abimbola POPOOLA

PRODUCTION AND CHARACTERIZATION OF CARBON BASED REFRACTORY FROM SPENT GRAPHITE ELECTRODE, OKPELLA KAOLIN AND IFON CLAY

[1.]Department of Metallurgical & Materials Engineering, Federal University of Technology, Akure, NIGERIA
[2.]Department of Chemical, Metallurgical & Materials Engineering, Tshwane University of Technology, Pretoria West, SOUTH AFRICA

Abstract: Clay-bond carbon refractory was produced from spent graphite, Ifon clay and Okpella kaolin. The effects of sintering temperatures on the phases developed and the physico-mechanical properties of the clay-bond carbon refractory produced was investigated. The raw Ifon clay, kaolin and graphite of predetermined mineralogical contents were used. Varied volume percentages of kaolin and graphite were thoroughly blended with 40 vol. % Ifon clay in a ball mill. The test samples that contain homogeneous mixture of raw materials were produced via uniaxial compaction. The compacted samples were subjected to firing at 800˚C, 900˚C, 1000°C and 1100˚C held for an hour. The sintered samples were characterized using x-ray diffractometry analysis. Various physical and mechanical properties were also determined using the ASTM standard. The results from the x-ray diffractometry showed the amount of mullite in the sample increased with increased sintering temperature and that corundum is formed at 800°C due to the presence of feldspar the raw materials used to produce the samples. It was also observed that increase in sintering temperature of the samples leads to reduction in the amount of quartz contents of the samples due to reaction of the quartz with corundum to form mullite. Increase sintering temperature resulted into decrease in apparent porosity and water absorption of the sintered samples while bulk density of the sample increased with increased sintering temperature. It was concluded that the sinusoidal relationship of the mechanical properties with the sintering temperature is due to co-existence of quartz and cristobalite in some of the samples.
Keywords: cabon refractory, mullite, corundum, sintering temperature, graphite

1. INTRODUCTION

The importance of refractory linings in technological advancement cannot be over emphasized. It is the development of a means of conserving the heat energy applied in the metallurgical process and holding the resulting molten alloy in molten form prior to casting into the require shapes that paved way technological advancement [1]. According to Semler [2], the refractory industry developed and flourished as a direct result of the need for heat resistant materials, to contain and control the thermal/chemical manufacturing processes of many industries. This implies that refractory lining is very important for the efficient operations of most industries. Refractories are utilized in large quantities in the metallurgical, glassmaking, and ceramics industries, where they are formed into a variety of shapes to line the interiors of furnaces, kilns, and other devices that process materials at very high temperatures [3-5]. Refractory materials are very useful and play very crucial roles in the industrial development of any nation. Despite the huge amount of clay deposits available in Nigeria and the enormous reported research that have been carried out in the development of refractory products, refractory industries are yet to spring up in the country. Nigeria continues to depend on external sources of refractory materials for many of its industries [6, 7].

Recently, the government of this country (Nigeria) has adopted a policy with the ultimate aim of encouraging production of automobile locally; this may be elusive without resuscitating our iron and steel industry. To achieve this, the importance of production of refractory lining locally cannot be over emphasized. This country is spending a lot of foreign exchange in importing refractories [8, 9], when there is abundant raw materials that needed to be processed to produce refractories of consistent physical and mechanical properties [10].

The motivation for this work is the abundant deposits of clay minerals which are readily available [11] and the existence of graphite deposit in Taraba State, one of the States in the north-eastern region of the country [10], in addition to readily available graphite from spent electrode. The primary aim of this work is to explore the evolution of phases in the carbon-mullite refractory and how these phases affect the mechanical properties of the refractory ceramic produced from the local deposit.

2. MATERIALS AND METHODS

— Materials

The materials utilized in this research work are, kaolin clay from a kaolin deposit in Okpella, Edo state, Nigeria, potter's clay from Ifon, Ondo State, Nigeria and spent graphite electrode (SGE) sourced from Pascal Chemicals, Akure, Ondo State, Nigeria.

— Clay processing procedure

This clay samples as obtained was soaked in water for three days to dissolve the clay and at the same time to form slurry. The resulting slurries were then sieved to remove dirt and other foreign substances using a sieve. These were then allowed to settle down for seven days after which the floating clear liquids were decanted. The settled fine clays is then poured into Plaster of Paris (P.O.P) moulds and left undisturbed for three days in other to allow the liquid present to drain out completely. The resulting plastic clay mass were sun dried and subsequently dried in a laboratory oven at 110°C for 24 hours to remove moisture content completely. The resulting dried clay samples were milled at 300 rev/ min for 4 hour to an average particle size of about 300µm.

— Powder Blending

The mass percent of the composition shown in Table 1(a) below was computed using Equations (1) and (2) [12] (Aramide *et al.* 2014) using the densities in Table 1(b) and the individual powders volume fraction in each composition. The powders were weighed per batch of 50.00 g on a sensitive electronic weighing balance to five (5) decimal places. The individual (batch) composition was thoroughly mixed in a ball mill for 4 hours at a speed of 72 rev/min. The compositions of the blended samples were shown in Table 1(a).

Table 1(a). Compositions of samples produced used

Sample	Kaolin clay (Vol. %)	Graphite (Vol. %)	Ifon clay (Vol. %)
D	50%	10%	40%
E	40%	20%	40%
F	30%	30%	40%

Table 1(b). Densities of components

Material	Kaolin Clay*	Graphite*	Ifon Clay*
Density (g/cm^3)	2.60	2.09	1.20

*As determined in the laboratory

If

$$M_T = V_{cl}\rho_{cl} + V_g\rho_g + V_K\rho_K \quad (1)$$

where V_{cl}, V_G, and V_K are respectively the volume fraction of Ifon clay, graphite and Okpella kaolin, ρ_{cl}, ρ_G and ρ_K are respectively the volume fraction of clay, graphite and Okpella kaolin, and M_T is the total mass contribution of all the components.

And if M is the mass of each batch, then the mass contribution of each component could be calculated from:

$$M_C = \frac{V_C\rho_C \text{ X } M}{M_T} \quad (2)$$

M_C is the mass contribution of a component in a batch (Ifon clay or graphite or Okpella kaolin), V_C, ρ_C the respective volume fraction and density of the component.

The resulting homogenous powder mixtures were compacted uniaxially into standard sample dimensions for cold crushing strength, bulk density and apparent porosity. The resulting green compacts were fired at varied temperatures (800°C, 900°C, 1000°C and 1100°C) in an electric furnace. The sintered samples were then characterized for various mechanical properties as described below.

— Chemical & mineralogical composition of the spent graphite electrode, Okpella kaolin and Ifon clay samples

The compound present in the clay samples were determined by x-ray fluorescence (XRF). The results obtained are presented in Table 2. The mineralogical phases present in all the samples were also determined using x-ray diffractometry (XRD). The phases present are reported in Figure 1 and Table 3.

Ultra high resolution field emission scanning electron microscope (UHRFEGSEM) equipped with energy dispersive spectroscopy (EDS) was used to examine the microstructure of the Ifon clay sample. The observed microstructures are presented in Figures 2.

Table 2: XRF Semi-quantitative analysis of the elements of Ifon clay sample (weight %)

Phases	Al_2O_3	SiO_2	Fe_2O_3	K_2O	MgO	CaO	Na_2O	TiO_2	Zr	Total
Ifon Clay	22.42	63.35	6.109	2.878	1.351	0.689	0.789	0.923	0.045	99.1

Table 3: XRD result of the Ifon clay, Okpella kaolin and Spent Graphite Electrode samples showing the quantity of phases

Identified Phases	Ifon Clay	Okpella Kaolin	Spent Graphite Electrode
Kaolinite	5.63	63.23	-
Microcline	30.90	-	-
Muscovite/illite	3.81	-	-
Plagioclase albite	18.22	-	-
Quartz	41.42	0.65	-
Graphite	-	-	44.2
Amorphous	-	36.12	55.8

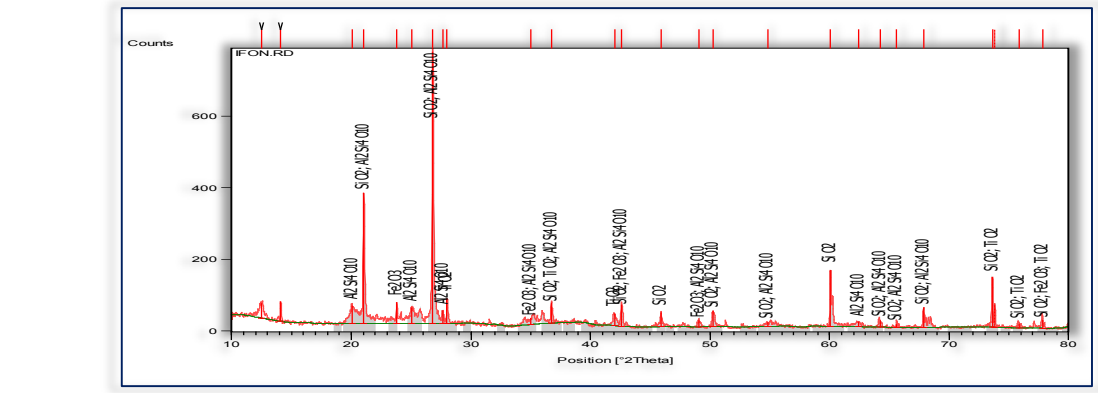

(a)

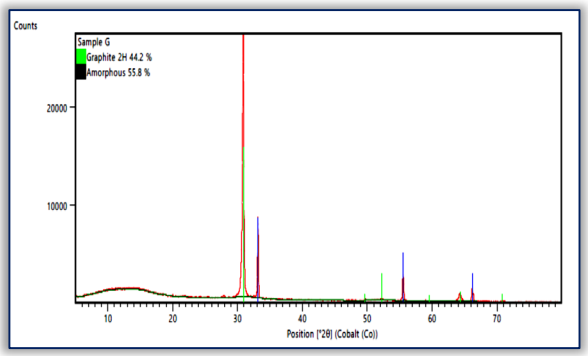

(b)

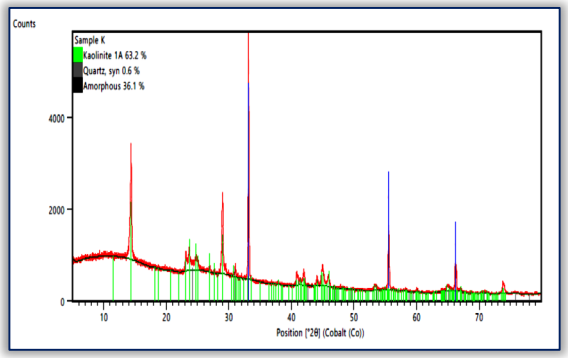

(c)

Figure 1: X-ray diffraction pattern (phase analysis) of the (a) Ifon clay sample, (b) Spent Graphite Electrode sample and (c) Okpella Kaolin sample

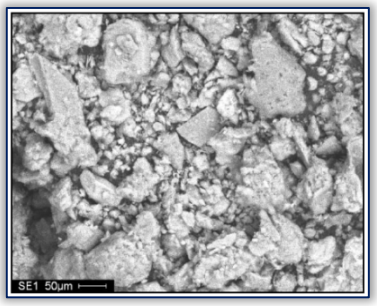

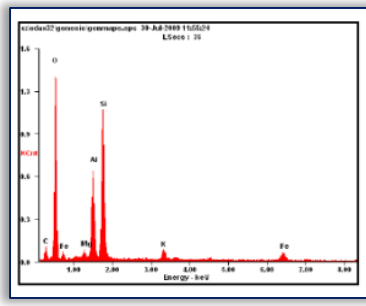

Element	Weight (%)
C	10.106
O	45.779
Mg	00.91
Al	11.736
Si	21.348
K	02.003
Fe	06.702

Figure 2. Typical SEM/EDS micrographs of Ifon clay sample

3. TESTING

— Apparent Porosity

Test samples from each of the ceramic composites were dried for 12 hours at 110°C. The dry weight of each fired sample was taken and recorded as D. Each sample was immersed in water for 6 hrs to soak and weighed while been suspended in air. The weight was recorded as W. Finally, the specimen was weighed when immersed in water. This was recorded as S. The apparent porosity was then calculated from the expression:

$$p = \frac{(W-D)}{(W-S)} \text{ x } 100\% \quad (3)$$

— Cold Compression Strength, Modulus of Elasticity and Absorbed Energy

Cold compression strength test is to determine the compression strength to failure of each sample, an indication of its probable performance under load. The standard ceramic samples were dried in an oven at a temperature of 110°C, allowed to cool. The cold compression strength tests were performed on INSTRON 1195 at a fixed crosshead speed of 10mm min-1. Samples were prepared according to ASTM C133-97 (ASTM C133-97, 2003) and cold crushing strength, modulus of elasticity and absorbed energy of standard and conditioned samples were calculated from the equation:

$$CCS = \frac{\text{Load to Fracture}}{\text{Surface Area of Sample}} \quad (4)$$

— Bulk Density

The test specimens were dried at 110°C for 12 hours to ensure total water loss. Their dry weights were measured and recorded. They were allowed to cool and then immersed in a beaker of water. Bubbles were observed as

the pores in the specimens were filled with water. Their soaked weights were measured and recorded. They were then suspended in a beaker one after the other using a sling and their respective suspended weights were measured and recorded. Bulk densities of the samples were calculated using the formula below:

$$\text{bulk density} = \frac{D}{(W-S)} \quad (5)$$

where: D = weight of dried specimen, S = weight of dried specimen suspended in water, and W = weight of soaked specimen suspended in air.

— Water Absorption Test

Water absorption tests were carried out following standard procedures. Samples were oven dried before weighing and the weights recorded were reported as the initial weight of the composites. The samples were then placed in distilled water maintained at room temperature (25°C) and at time intervals of 24h, the samples were removed from the water, cleaned using a dry cloth and weighed. The weight measurements were taken periodically at time intervals of 24h. The amount of water absorbed by the composites (in percentage) was calculated using the equation:

$$W = \frac{(W_T - W_O)}{W_O} \quad (6)$$

4. ANALYSIS

— Qualitative and Quantitative XRD

The samples were prepared for XRD analysis using a back loading preparation method [13, 14, 15]. They were analysed using a PANalytical X'Pert Pro powder diffractometer with X'Celerator detector and variable divergence- and receiving slits with Fe filtered Co-Kα radiation. The phases were identified using X'Pert Highscore plus software. The receiving slit was placed at 0.040°. The counting area was from 5 to 70° on a 2θ scale. The count time was 1.5 s. The temperature-scanned XRD data were obtained using an Anton Paar HTK 16 heating chamber with Pt heating strip. Graphical representations of the qualitative result follow below.

The relative phase amount (weight %) was estimated using the Rietveld method (Autoquan Program) as reported by Young et al. (1994) [16].

— Scanning Electron Microscopy

Morphology and microanalysis of the clay and composite samples were determined using ultrahigh resolution field emission scanning electron microscope (UHR-FEGSEM) equipped with energy dispersive spectroscopy (EDS). The pulverized clay samples/sintered ceramic composite samples were previously gold coated. The samples were studied using ultra-high resolution field emission scanning electron microscope (UHR-FEGSEM) equipped with energy dispersive spectroscopy (EDS). Particle images were obtained with a secondary electron detector.

— X-Ray Fluorescence (XRF)

The major elements were determined by X-ray fluorescence with an ARL® 9800 XP spectrometer. The pulverized clay samples were mixed with lithium tetraborate for chemical analysis. The ignition loss was measured by calcinations at 1000°C.

5. RESULTS & DISCUSSIONS

Table 2 shows the x-ray fluorescent semi-quantitative analysis results of the Ifon clay sample, Table 3, Figure 1 (a), (b), (c), and Figure 2 show the x-ray diffractometry analysis results of the Ifon clay, Opella kaolin and spent graphite electrode samples used in the research work. Table 4 and Figures 3 to 9 show the effects of sintering temperatures on the phase developments in the various ceramic samples.

Table 4: Qualitative and Quantitative XRD results of the Various Samples

	Quartz	Graphite	Corundum	Microcline	Hematite	Anorthite	Muscovite	Mullite	Cristobalite	Amorphous
FT1	21.34	11.75	0.8	4.19	0	0.9	trace	0.84	0	60.17
FT2	23.07	16.44	0.28	3.81	0.05	1.01	trace	3.79	0.05	51.52
FT3	20.66	11.66	1.95	2.72	0	0.59	trace	5.17	0	57.24
FT4	20.14	11.34	0.66	0.65	0	0.06	trace	16.58	5.46	45.1
DT1	21.69	7.39	0.6	4.4	0.1	1.04	0.2	0.07	0	64.51
DT2	21.44	6.09	0.61	4.82	0.03	1.88	trace	0	0	65.13
DT3	18.79	9.06	1	2.83	0	0.27	trace	5.87	0	62.19
DT4	18.26	8.72	0.79	0.86	0	0	trace	16.51	5.89	48.98
ET1	23.63	10.49	1.07	5.47	0	1.66	trace	0.88	0	56.79
ET2	24.05	9.05	1.1	5.14	0	1.43	trace	1.93	0	57.3
ET3	23.12	11.53	2.56	3.06	0	0.97	trace	6.93	0.21	51.62
ET4	21.07	10.53	0.96	0.7	0	0	trace	17.86	5.83	43.04

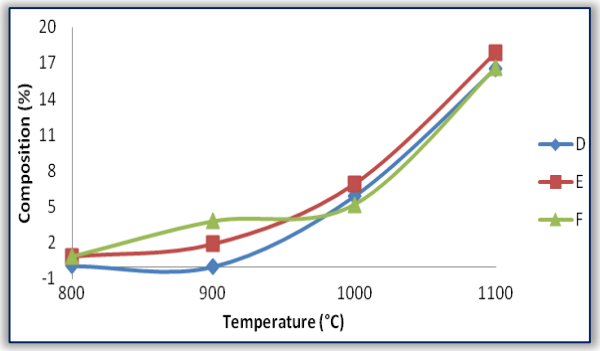

Figure 3. Effects of Sintering Temperatures on Mullite Development in the Samples

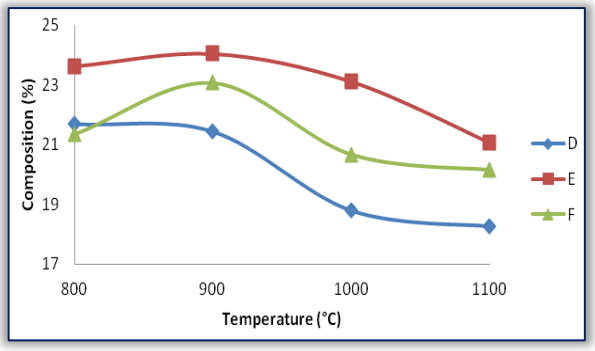

Figure 4. Effects of Sintering Temperatures on the quartz content of the Samples

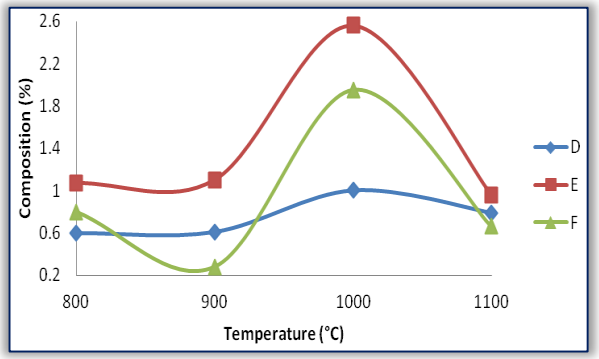

Figure 5. Effects of Sintering Temperatures on the Corundum content of the Samples

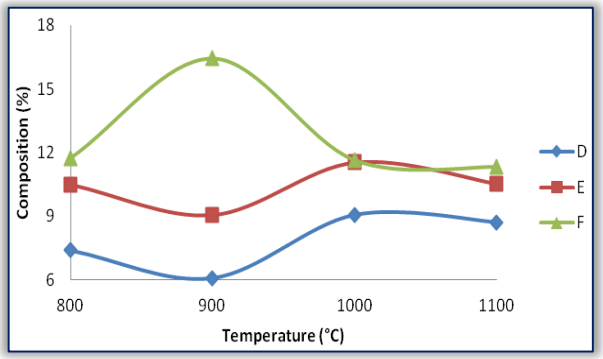

Figure 6. Effects of Sintering Temperatures on the Graphite content of the Samples

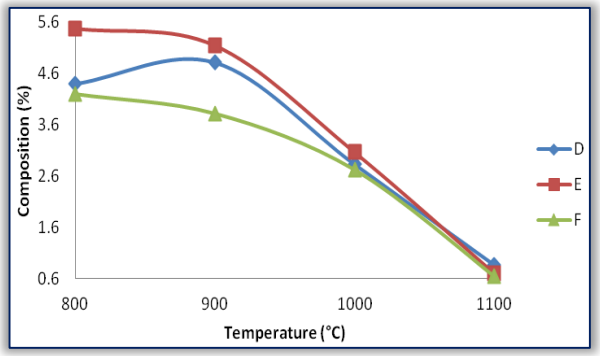

Figure 7. Effects of Sintering Temperatures on the Microcline content of the Samples

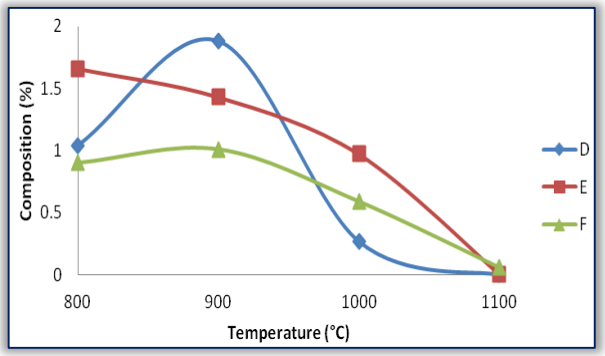

Figure 8. Effects of Sintering Temperatures on the Anorthite content of the Samples

— Effects of Sintering Temperatures on Phase Development in the Various Ceramic Samples

≡ Mullite

From Table 4 and Figure 3 the effect of sintering temperatures on the phase developments in the various ceramic samples is clearly depicted. Comparing the phase constituents of the sintered ceramic samples with those of the raw materials (see Table 3 and Figure 1) used in preparing the samples, it will be observed that the major phase constituent that was formed as a result of increased sintering temperature is the mullite. Mullite was not in the raw materials; it will be observed that generally the amount of mullite formed in the sample increased with increased sintering temperature. It is an established fact that kaolinite undergoes various phase transformations with increased sintering temperatures from dehydroxilation to meta-kaolinite formation and

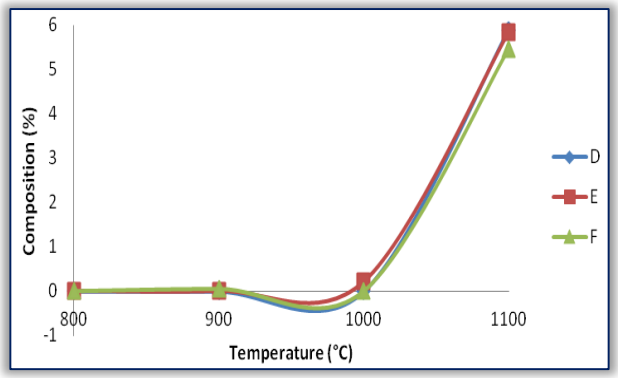

Figure 9. Effects of Sintering Temperatures on the Cristobalite content of the Samples

eventually to mullite formation with excess silica [1, 12, 17, 18]. This explains the reason why the kaolinite observed in the raw Okpella kaolin and Ifon clay disappeared in the sintered samples and mullite is observed.

≡ Quartz and Corundum

From Table 4 and Figure 4 the effect of sintering temperature on the quartz content of the various ceramic samples is shown. It is observed that the quartz content of the samples decreased with increased sintering temperature. One cold suggest that the quartz was being consumed with increased sintering temperature as a reactant. Comparing with Figure 5, which show the sintering temperature on the corundum (alumina; Al_2O_3) content of the various ceramic samples, it is observed that the corundum content of the ceramic samples slightly increased (except for sample F, which decreased) as the sintering temperature increased from 800°C to 900°C, further increase in the sintering temperature 1000°C resulted to increased corundum contents for all the samples (samples D, E and F) while further increase in the temperature lead to decrease in the corundum contents. Many researchers have reported that kaolinite form meta-kaolinite between 420°C to 660°C which at around 900°C breaks down to amorphous silica and γ-Al_2O_3-type spinel [12, 17, 18]. They further stated that, at 1100°C the γ-Al_2O_3 and silica recrystallize to form mullite. This explains the reason for the progressive decrease in the quartz contents with increased sintering temperature. Furthermore, the silica formed during the decomposition of meta-kaolinite is amorphous, which is not detected by the x-ray diffractometry analysis, this means that the silica that reacted with the Al_2O_3 to form mullite is from the quartz.

Moreover meta-kaolinite was not detected by the x-ray diffractometry analysis at 800°C, but the corundum was observed at 800°C, which increased as the sintering temperature increased to 900°C. It could be inferred that meta-kaolinite decomposition to corundum starts and complete below 800°C while crystallization of the corundum continues up to 1000°C. The depletion of meta-kaolinite below 800°C could be due to the presence of feldspar in the raw Ifon clay used as binder.

≡ Graphite

Figure 6 shows the effects of sintering temperature on the graphite content of the various ceramic samples. From the figure and Table 4, it is observed that the graphite content of samples D at various sintering temperatures has the least values, follow by samples E, while samples F has the highest graphite content values. Comparing this with Table 1(a) it is observed that trend is in order; the amount of graphite used producing the samples, D contain the least amount of graphite (10%) follow by E (20%) and then F (30%). But it is observed that the contents of graphite in the sintered samples are much lower than those used in producing them. There are two explanations for this; on one hand, it could be explained that it is due to the crystalline graphite content of the raw graphite used (44.2% graphite and 55.8% amorphous). Since the xrd only characterized the crystalline contents, hence the lower contents of the graphite. On the other hand, it is a well-known fact that at above 900°C graphite is prone to oxidation by reaction with oxygen in the furnace atmosphere, thereby producing carbon-dioxide; this will lead to increase in porosity of the sample. Comparing this with Table 5(b) and Figure 10, it will be observed that sample D generally has the highest porosity while sample E and F are within the same range.

≡ Microcline and Anorthite

From Figures 7 and 8, the effects of sintering temperatures on the microcline and anorthite contents of the samples are clearly depicted. From Figure 7, it is observed that the microcline content of the samples decreased with increase in sintering temperature. Similarly, from Figure 8 it is observed that the anorthite contents of the samples decreased with increase in the sintering temperature. From both figures, it is equally observed that the contents of both the microcline and the anorthite are minima at 1100°C. This behavior agrees with the findings of Conconi *et al*. [19], that microcline disappears beyond 1100°C. Moreover, both the anorthite and microcline are feldspars, it has been reported that high temperature x-ray crystallographic studies of alkali feldspar shows that continuous changes occur as a function of increasing temperature [20].

Furthermore, from Table 3, it is observed that raw clay used in producing the samples does not contain anorthite, but it contains plagioclase/albite. From the results of the xrd (Table 4) of the sintered samples, it is equally observed that the plagioclase/albite is conspicuously missing in the crystalline phases detected. This could be explained that the plagioclase/albite undergoes some transformations/ reactions to form anorthite as the samples were sintered [21]. It is noteworthy that both the anorthite and microcline disappear at 1100°C and at the same temperature mullite contents of the sintered samples increased sharply (Figure 3). Similarly at this same temperature the contents of cristobalite (Figure 9) in the sintered samples increased from nearly zero percent to between 5 and 6%. It could be reasonably inferred that the microcline and the anorthite were consumed as reaction reactants yielding more mullite and cristobalite (excess silica) at around 1100°C.

— Effects of Sintering Temperature on the Physical and Mechanical Properties of the Samples

Table 5 (a) and (b) with Figures 10 to 15 show the effects of sintering temperature on various physical and mechanical properties of the sintered samples.

≡ Effects of Sintering Temperature on the Physical Properties of the Samples

Table 5(b) and Figures 10 to 12 show the effects of sintering temperature on various physical properties of the sintered samples.

Table 5(a). Effects of sintering temperatures on the mechanical properties of the various samples

Temperature (°C)	Sample D			Sample E			Sample F		
	Cold Crushing Strength (MPa)	Young's Modulus (MPa)	Absorbed Energy (J)	Cold Crushing Strength (MPa)	Young's Modulus (MPa)	Absorbed Energy (J)	Cold Crushing Strength (MPa)	Young's Modulus (MPa)	Absorbed Energy (J)
800	11.0639	201.0156	4.41547	12.44362	144.2237	6.30235	9.64851	171.8039	3.6829
900	4.3959	63.2137	1.8639	3.6690	67.1000	1.4815	7.2452	166.479	3.06246
1000	3.1849	58.257	1.2125	15.8283	183.473	8.7757	13.6059	153.721	7.22528
1100	19.6821	302.476	10.4134	6.4695	81.6654	3.2568	8.3092	184.609	3.97382
1200	2.7846	83.1732	0.73096	18.0016	358.527	7.7876	9.0802	234.691	3.50318

≡ Apparent Porosity

From Figure 10 and Table 5(b) the effect of sintering temperature on the apparent porosity of the various sintered sample is clearly seen. It is broadly observed that the apparent porosity of the sintered samples decreased with increased sintering temperature. This is expected as the sintering temperature is increased, more liquid phase is formed which closed up the voids (pores) within the ceramic body thereby reducing the porosity.

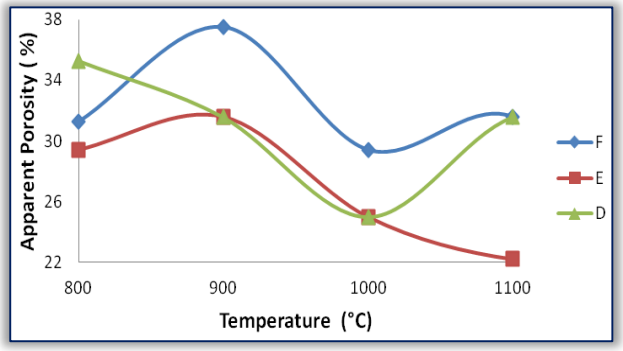

Figure 10: Effects sintering temperature on apparent porosity of the samples

≡ Bulk Density

From Figure 11 and Table 5(b) the effect of sintering temperature on the bulk density of the various sintered sample is clearly seen. It is broadly observed that the bulk density of the sintered samples increased with increased sintering temperature.

This could be explained that the samples become denser with increased sintering temperature due to the closing up of more of the interparticle voids within the ceramic samples as earlier explain in the preceding section. This eliminates more air with the samples and replaced them with more dense vitreous/glassy ceramic material.

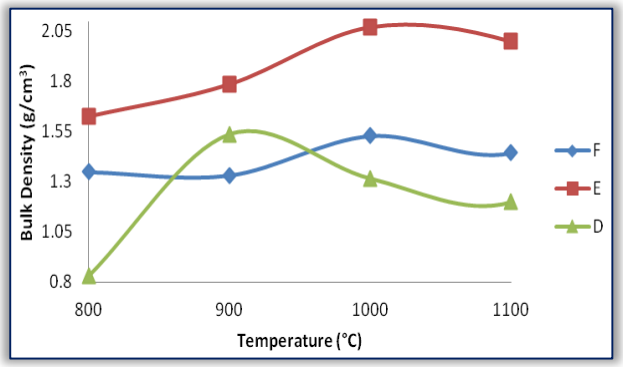

Figure 11. Effects sintering temperature on bulk density of the samples

≡ Water Absorption

From Figure 12 and Table 5(b) the effect of sintering temperature on the water absorption of the various sintered sample is clearly seen. It is broadly observed that the water absorption of the sintered samples decreased with increased sintering temperature. This is similar to the behavior of the apparent porosity with the increased sintering temperature.

It is because the water absorption is directly related to the open porosity within the ceramic sample. This means that the open porosity also reduced with increased sintering temperature.

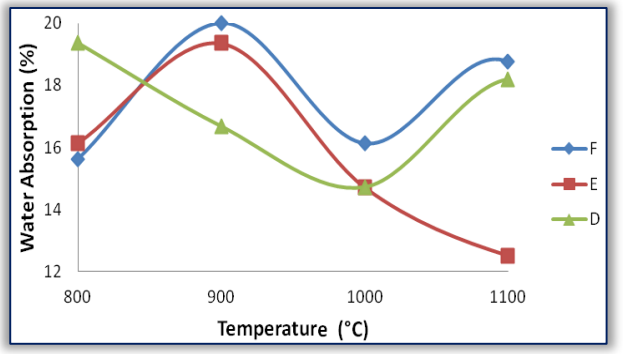

Figure 12. Effects sintering temperature on water absorption of the samples

— Effects of Sintering Temperature on the Mechanical Properties of the Samples

Table 5(a) and Figures 13 to 15 show the effects of sintering temperature on various mechanical

properties of the sintered samples. Figure 13 show the effect of sintering temperature on the cold crushing strength of the sintered samples. From the Table and the figure, it is observed that the cold crushing strength of the various samples initially decreased with increasing sintering temperature from 800°C to 900°C. Further increase in the sintering temperature to 1000°C lead to different response from samples E and F (which increased with the increased sintering temperature) while sample D further decreased in its value of cold crushing strength. As the sintering temperature in further increased from 1000°C to 1100°C the values of the cold crushing strengths of samples E and F decreased, while that of the sample D increased. This various responses of the cold crushing strength of the samples to the sintering temperature cannot be unconnected with the responses of their apparent porosities and bulk densities to the sintering temperature.

Table 5(b) Effects of sintering temperatures on the physical properties of the various samples

	Sample D			Sample E			Sample F		
Temperature (°C)	Porosity (%)	Water Absorption (%)	Bulk Density (g/cm³)	Porosity (%)	Water Absorption (%)	Bulk Density (g/cm³)	Porosity (%)	Water Absorption (%)	Bulk Density (g/cm³)
800	35.29412	19.35484	0.83333	29.41176	16.12903	1.6250	31.2500	15.625	1.3500
900	31.57895	16.6667	1.538462	31.57895	19.35484	1.785714	37.500	20.000	1.33333
1000	25.0000	14.7058	1.318182	25.0000	14.70588	2.07143	29.41176	16.1290	1.529412
1100	31.57895	18.1818	1.2000	22.22222	12.5000	2.000	31.57895	18.7500	1.444444
1200	31.57895	16.2162	1.722222	22.22222	11.76471	1.666667	22.22222	12.1212	1.8125

Comparing the Figure 13 with Figures 10 and 11, it will be observed that where the apparent porosity increased with increased sintering temperature, the cold crushing strength decreased and vice versa. This is because increase in porosity with sintering temperature means less matter will be available to carry the load [17].

Furthermore, comparing this with Table 4, it will be observed that the cold crushing strength is lower where quartz and cristobalite (different phases of silica) co-exist. It could be said the lower mechanical property observed is as a result of thermal stress due to differential thermal expansion of the different phases. The bulk of this quartz is introduced by the Ifon clay used as binder in the samples.

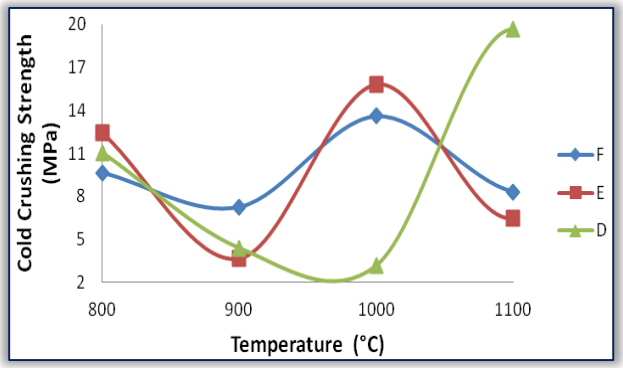

Figure 13. Effects sintering temperature on cold crushing strength of the samples

Figures 14 and 15 show the effects of sintering temperature on the Young's modulus of elasticity and the absorbed energy of the various samples. It is observed that the responses of the concerned properties with the sintering temperature follow the same pattern with that of the cold crushing strength. It is because cold crushing strength of a material (just like tensile strength) is related to its Young's modulus and absorbed energy. The same explanation given above for cold crushing strength is applicable for Young's modulus and absorbed energy also.

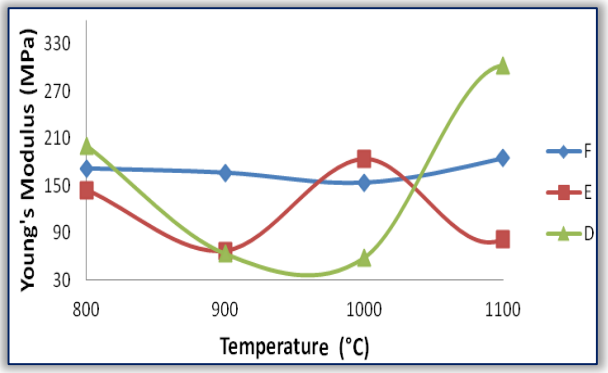

Figure 14. Effects sintering temperature on Young's modulus of elasticity of the samples

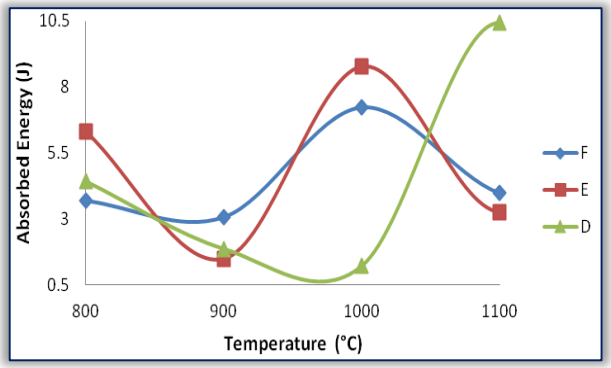

Figure 15. Effects sintering temperature on absorbed energy of the samples

6. CONCLUSIONS

From the conclusion so far, it is concluded that;

- the amount of mullite formed in the sample increased with increased sintering temperature;
- corundum is formed at 800°C due to the presence of feldspar in one of the raw materials used to produce the samples;
- increase in sintering temperature of the samples leads to reduction in the amount of quartz contents of the samples due to reaction of the quartz with corundum to form mullite;
- increase sintering temperature resulted into decrease in the apparent porosity and the water absorption of the sintered samples while the bulk density of the sample increased with increased sintering temperature;
- the sinusoidal relationship of the mechanical properties with the sintering temperature is due to co-existence of quartz and cristobalite in some of the samples sintered at different temperature;

References

[1] Aramide F.O., Seidu S.O. Production of refractory lining for diesel fired rotary furnace, from locally sourced kaolin and potter's clay, Journal of Minerals and Materials Characterization and Engineering, 1, 2013, 75-79.
[2] Semler C.E., "Steel Industry—Status and Changes," Refractories Applications and News, 10(2), 2005, 7-9
[3] Aramide F.O., Oke S.R. Production and Characterization of Clay Bonded Carbon Refractory from Carbonized Palm Kernel Shell, ACTA TEHNICA CORVINIENSIS – Bulletin of Engineering, Tome VII, Fascicule 4 [October – December], 2014, p. 133-140, ISSN: 2067 – 3809
[4] Yami A.M., Umaru S. Characterization of some Nigerian Clays as Refractory Materials for Furnace Lining, Continental J. Engineering Sciences, 2007, pp. 30-35.
[5] Abolarin, M.S., Olugboji, O.A., Ugwoke, I.C., Experimental investigation on local refractory materials for furnace construction, 5th Annual Engineering Conference Proceedings, 2004, 82-85.
[6] Oyetunji A., Opaluwa I., Study the Compressive Strength of Produced Sand Cores Using Clay and Starch as Binder for the Casting of Aluminium Alloy T-Joint pipe. International Research Journal of Engineering and Technologies, 4(3), 2012, 50-60.
[7] Musa U., Aliyu M.A., Mohammed I.A., Sadiq M.M., A Comparative Study on the Refractory Properties of selected Clays in North Central Nigeria. Academic Research International, 3(1), 2012, 393-398.
[8] Osarenmwinda J.O., Abel, C.P., Performance Evaluation of Refractory Bricks produced from locally sourced Clay Materials, J. Appl. Sci. Environ. Manage. 18(2), 2014, 151-157
[9] Aye E.A., Oyetunji A., Metallurgical Analysis of Ugunoda Clay Deposit, Nigeria for Use as a Refractory International Journal of Science and Advanced Technology 3(10), 2013, 25-29
[10] Ibrahim H.D., Biliaminu K.O., Steel Raw Materials in Nigeria, Raw Materials Research and Development Council, Abuja, 2010, 79-84
[11] Borode, J.O., Onyemaobi, O.O., Omotoyinbo. J.A., Suitability of Nigerian clays as refractory raw materials. Nigerian Journal of Engineering Management 3, 2000, 14–18.
[12] Aramide F.O., Alaneme K.K., Olubambi P.A., Borode J.O., Effects of 0.2Y-9.8ZrO_2 Addition on the Mechanical Properties and Phase Development of Sintered Ceramic Produced from Ipetumodu Clay, ANNALS of Faculty Engineering Hunedoara– International Journal of Engineering, Tome XII, Fascicule 4 [November], 2014, p. 343-352, ISSN: 1584-2673.
[13] Aramide F.O., Effects of Sintering Temperature on the Phase Developments and Mechanical Properties Ifon Clay. Leonardo Journal of Sciences, Issue 26 (January-June), (14), 2015, p. 67-82.
[14] Aramide F.O., Alaneme K.K., Olubambi P.A., Borode J.O., Characterization of some clay deposits in South West Nigeria, Leonardo Electronic Journal of Practices and Technologies, Issue 25 (July-December), (13), 2014, p. 46-57.
[15] Kleeberg R., Monecke T., Hillier S., Preferred orientation of mineral grains in sample mounts for quantitative XRD measurements: How random are powder samples?, Clays and clay minerals, 56 (4), 2008, p. 404-415.
[16] Young R.A, Sakthivel A., Moss T.S., Paiva-Santos C.O., Rietveld analysis of X-ray and neutron powder diffraction patterns, School of physics, Georgia Institute of Technology, 1994, Atlanta, U.S.A.
[17] Aramide, F.O., Production and Characterization of Porous Insulating Fired Bricks from Ifon Clay with Varied Sawdust Admixture. Journal of Minerals and Materials Characterization and Engineering, 11, 2012, 970-975.
[18] Qiu, G; Jiang, T; Li, G; Fan, X., Huang, Z., Activation and removal of silicon in Kaolinite by thermochemical process, Scan. J. Metallurgy, 33, 2004, 121-128.
[19] Conconi M.S., Gauna M.R., Serra M.F., Suarez G., Aglietti E.F., Rendtorff N.M., Quantitative firing transformations of a triaxial ceramic by X-ray diffraction methods, Cerâmica 60, 2014, 524-531
[20] Grove T.L., Hazen R.M., Alkali Feldspar Unit-Cell Parameters at Liquid Nitrogen Temperatures: Low Temperature Limit of the Displacive Transformation, American Mineralogist, 59, 1974, p1327-1329.
[21] Julian R.G. Review of the behavior of plagioclase under metamorphic conditions American Mineralogist, 67, 1982, p 643-652